2020 Building Performance Analysis Conference and
SimBuild co-organized by ASHRAE and IBPSA-USA

NUMERICAL INVESTIGATION OF EXTERNAL CONVECTIVE HEAT TRANSFER COEFFICIENT FOR BUILDINGS IN DIFFERENT LAND-USE CLASS

Anwar D. Awol[1], Girma T. Bitsuamlak[1], and Fitsum A. Tariku[2]
[1]Univeristy of Western Ontario, London, ON, Canada
[2]British Colombia Institute of Technology, BC, Canada

ABSTRACT

Convective heat transfer coefficient (CHTC) is known to play an important role in the evaluation of heat exchange between a building and its surroundings. There are several correlations suggested for the estimation of CHTC from the external surfaces of a building. However, there is a marked difference between values obtained from these correlations under similar set of conditions. Therefore, there is a need for an extensive correlation addressing the discrepancies in some of the existing correlations. In the current study, the impact of built morphology, associated with different land-use classes (e.g., industrial, residential, or downtown, etc.), on the convective heat transfer from buildings is numerically investigated. CFD simulations are conducted in a Navier-Stokes solver with Reynolds stress turbulence model as a closure method. The surrounding buildings are expected to influence the local microclimate (wind speed and turbulence), which in turn will affect the CHTC of the study building. Arrays of building-like bluff bodies from different land-use class with several packing density representing different flow regimes, and a benchmarking isolated cube case, have been investigated. Frontal/planar densities of sections of various parts of cities, based on their land-use class - from literature, are used to relate CHTC findings from simulation to land-use classifications. The results indicate that the behavior of convective heat transfer from building surfaces significantly depends on the land-use class designation of the location of the study building. The development of land-use class based CHTC correlations is expected to reduce the bias resulting from using correlation based exclusively on isolated building studies.

INTRODUCTION

The need for consideration of the influence of urban microclimate on CHTC from building surfaces has been argued in some studies (Moonen et al. 2012, Blocken et al. 2011, van Hoof et al. 2010). Chen et al. (2017) maintained the critical nature of this influence. The effect of the sheltering from neighboring buildings has been considered in site/configuration specific studies (Mirsadeghi et al. 2013, Allegrini et al. 2012, Liu et al. 2007). Awol et al. (2019) stated the significant scatter in some of the existing CHTC correlations have roots in the challenge of sufficiently addressing the microclimatic influences. Changes in CHTC are also reported by recent attempts to account for the impact of the height of buildings alone; by Montazeri et al. (2017) and Kahsay et al. (2018). Efforts have also been made to address the issue through a local velocity reference condition. The results of this effort also demonstrate discrepancy among reported estimates of CHTC (Ito et al. 1972, Sharples 1984, Loveday et al. 2004, Liu and Harris 2007).

The alteration that occurs to the local wind field is responsible for the changes that would arise on the CHTC from the building surfaces. The surrounding built arrangement (size, orientation, and packing), in turn, is responsible for the changes to the wind field. This has been recognized in several studies (Adamek et al. 2017, Awol et al. 2017, Coceal et al. 2006, Cheng et al. 2002, Macdonald 2000, Oke 1988). Several of the CHTC correlations in literature are obtained from laboratory and field studies (Evangelisti et al. 2017, Liu et al. 2007, Hagishima et al. 2003, Loveday et al. 1996, Sharples 1984, Sparrow et al. 1979, Ito et al. 1972). However, recently, validated CFD simulations have been used to successfully develop correlations for CHTC (Kahsay et al. 2018, Montazeri et al. 2017, Liu et al. 2013, Defraeye et al. 2010, Blocken et al. 2011, Blocken et al. 2009, Emmel et al. 2007). Further, Mirsadeghi et al. (2013), Defraeye et al. (2011), and Palyvos (2008) have conducted an extensive review of literature on external convective heat transfer coefficient.

Meinders (1998) conducted an experiment on a row of cubes to investigate the effect of neighboring obstacles on CHTC from a cube surface. Lui et al. (2013) examined the effect by considering a CFD study on 2D array of cubes. In a numerical study, Awol et al. (2019) have shown the effect of urban packing density on CHTC (from building surfaces) for homogenous packing densities, more specifically for cases with equal frontal and planar densities ($\lambda_f = \lambda_p$, i.e., cubical buildings). The frontal packing density (λ_f), planar packing density (λ_p) are expressed as;

$$A_D = \sum_1^n A_{d,i} \quad (1)$$

$$\lambda_f = \frac{\sum_1^n A_{f,i}}{A_D} = \frac{A_F}{A_D}, \qquad \lambda_p = \frac{\sum_1^n A_{p,i}}{A_D} = \frac{A_P}{A_D} \quad (2)$$

where $A_{f,i}$ is the frontal area per each building, $A_{p,i}$ is the planar, and $A_{d,i}$ is the unit underlying lot area on the ground surface per each building. The representative frontal and planar area densities at the neighborhood level are then found from the ratio of the total frontal (A_F) and the total top (A_P) surface areas for the total lot area, respectively.

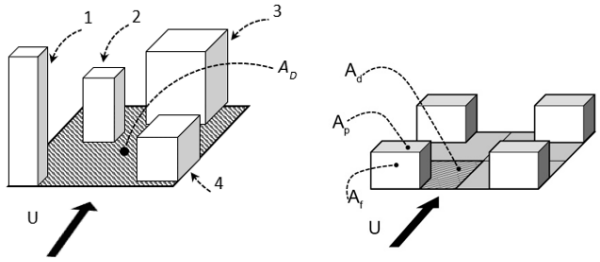

a) *b)*

Figure 1 Definitions of frontal and planar density a) the schematic heterogeneous form b) simplified homogeneous representation

Although the cubical building system may be a pragmatic first step idealization of the urban topology, it is an oversimplified one. Sets of more plausible, but still, homogeneous idealizations are examined in this study numerically. This paper presents two sets of CFD based investigations to assess (i) the effect of change in frontal density on CHTC of building surfaces by only varying λ_f while λ_p is fixed, and (ii) the effect of change in planar density by varying only λ_p while λ_f is fixed, respectively. An array of planar and frontal density pair are simulated from various representative flow regimes; that correspond to conditions in various land-use class designation. The same input conditions and the identical computational domain is set up for all cases, to limit the numerical effects on each simulation.

The test sets, the computational setup, the validation, and the results of the study are discussed in the following sections.

DESCRIPTION OF THE SIMULATED URBAN-LIKE SETUP

In this study, the nonhomogeneous urban topology (Figure 1a) is represented by an equivalent but simplified homogenous arrangement (Figure 1b). The equivalency is determined by maintaining equal frontal and planner density between the actual and simplified topology as defined in equations (1) and (2). The frontal and planar density parameters for nonhomogeneous urban packing density are described in Figure 1.

Set of densities considered

A planar-frontal density pair matrix is generated. The two sets of densities are generated corresponding to the two main objectives of the study, namely (i) effect of changing frontal density at a fixed planar density and (ii) effect of changing planar density at fixed frontal density.

More specifically, the impact of changes in (i) frontal density (λ_f) and (ii) planar density (λ_p) on CHTC from building surfaces are tested. Table 1 shows the test scenarios considered.

Table 1 The sets of simulations conducted based on constant λ_p or λ_f

λ_f	λ_p		λ_f	λ_p
0.01	0.01		0.15	0.15
0.02	0.02		0.175	0.02
	0.1			0.1
	0.175			0.175
0.025	0.025			0.25
0.05	0.02			0.3
	0.05		0.2	0.2
	0.1		0.225	0.225
	0.175		0.25	0.1
0.075	0.075			0.175
0.1	0.02			0.25
	0.5			0.3
	0.1		0.3	0.1
	0.175			0.175
	0.25			0.25
	0.3			0.3
0.125	0.125			

Computational domain, boundary conditions, and physics model

The representative urban density in each case is obtained from a hypothetical 2D array of buildings with 14 blocks in stream-wise and infinite size in transverse. For this type of arrangement, the representative simplified flow can be obtained from the simulation of a single longitudinal strip of the array. For this to be a sound representation, the two parallel planes normal to the transverse direction that is placed half spacing away from the selected row on either side need to be assumed planes of symmetry (as shown in Figure 2). The limits of the simulation domain are shown in Figure 2, and the dimensions are shown in Figure 3.

The choice of the blocks' dimensions is such that the same domain and boundary conditions are used for all computational simulations. Accordingly, the domain is set up for the highest density case considered, using Tominaga et al. (2008) and Franke et al. (2011).

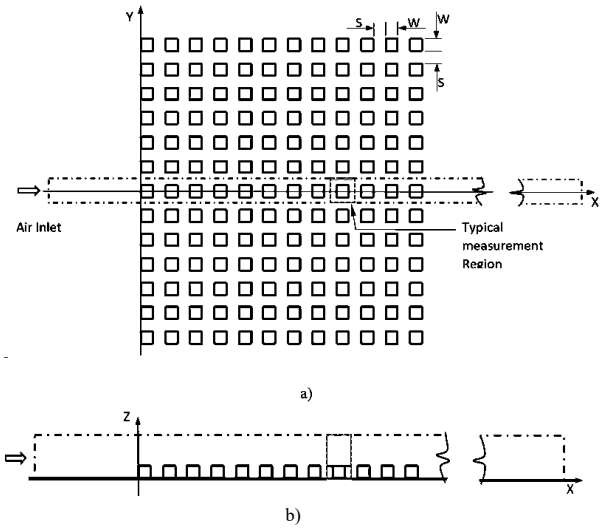

Figure 2 The building array with the study section (broken lines) and spacing parameters indicated on a) plan and b) elevation views.

The top surface of the domain is assumed as a symmetry plane. The bottom surface of the domain is set as an adiabatic no-slip wall. The block surfaces are wall boundaries at a uniform temperature of 30 °C. The outlet of the domain is assigned a pressure outlet boundary condition.

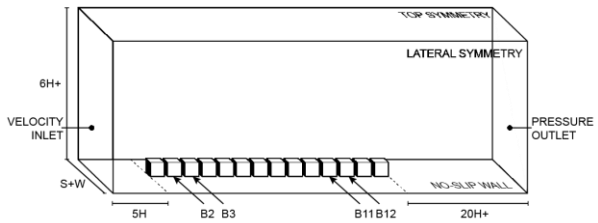

Figure 3 The computational domain, its dimensions and boundary conditions (H height of cubic = 21.25 m)

The inlet boundary is an atmospheric boundary layer wind extracted from Engineering Science Data Unit (ESDU). The mean velocity profile has a velocity $u_{10} \approx$ 4.7 m/s at 10 m height in an open terrain exposure condition (of aerodynamic roughness, z_0 = 0.01). The turbulence values applied at the inlet are the three principal components of the Reynolds stress tensor. These values are reduced from the components of turbulent intensity and length scale tensor values provided by ESDU. Figure 4 shows the mean velocity and the principal components of the Reynolds stress values implemented.

Approximately $1.5*10^6 – 2.5*10^6$ unstructured grid cells are generated. The grids are refined based on a volume around the blocks, the block surfaces, block edges, the wake region, and the computational domain wall boundary. Five prismatic layers of grids are applied near the wall boundaries (i.e., running parallel to each wall).

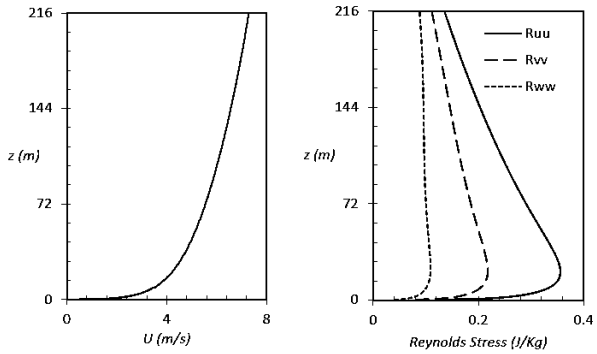

Figure 4 The inlet profiles of mean velocity and the principal components of Reynolds stress

An example of the computational grid used in one of the simulations is shown below (Figure 5).

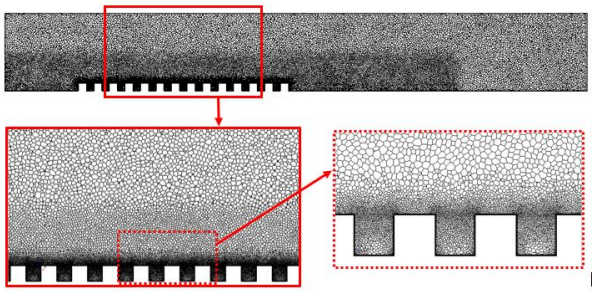

Figure 5 Elevation view of a sample mesh section

Steady Reynolds Averaged Navier-Stokes (RANS) and the energy equations are implemented to solve the problem in a CFD environment. The turbulence scheme used in the study is the second-moment closure method, Reynolds stress turbulence model (RSM). This method is important for flows where secondary flows and anisotropic turbulence are substantial (Speziale 1991, Murthy et al. 2008, Leschziner 1990, Launder et al. 1975). More information regarding this section can be found in Awol et al. (2019).

VALIDATION OF THE MODEL

The current CFD model is compared to the experimental findings of Merinders (1998) for validation purposes. First, the experiments from literature are briefly described, and second, the computational model that mimicked the experimental study is presented.

Meinders (1998) experiment was conducted in a chamber with a 500 mm x 50 mm test section. Nine cubes were aligned along the longitudinal flow direction and in the middle of the vertical channel wall. The cube size and the spacing between the cubes were 15 mm

each. The outer layer of the cube was a 1.5 mm epoxy shell, and a copper core formed the inner part of the cube. The copper core was maintained at a temperature of 75°C, and the conductivity of the epoxy material was 0.24 W/m.K.

An infrared camera was used to scan the external surfaces of the cubes to provide the temperature distribution. The temperature distribution is then used to calculate the convective heat transfer coefficient; after accounting for radiative losses from supply flux. The inlet was supplied with a bulk velocity of 5.1 m/s, corresponding to an approximate Reynolds number of 5065, based on the height of the cubes. The temperature of oncoming flow at the inlet was set at 21°C. Additional detail information can be found in Meinders (1998).

The computational model used for validation comprised a one to one scale replica of the tunnel section with the downstream fetch size of 20H to ensure the full inclusion of the downstream wake effects within the computational domain. Upstream fetch of 5H is considered, according to Tominaga et al. (2008), and Franke et al. (2011). The wall, on which the cubes are mounted, is oriented vertically to match the condition in the experiment, as shown in Figure 6. The properties of epoxy material are applied to the cubical shell model, to allow for the calculation of conduction heat transfer through the shell. The inner surface of all cube shells is set to be at a temperature of 75 °C. A temperature of 21 °C is applied to the incoming airflow. The outlet conditions are kept at zero pressure gradient. All lateral, top, and bottom faces of the computational domain are considered adiabatic, no-slip wall boundaries. The outer surfaces of the cubes are set as no-slip walls and with non-adiabatic environmental conditions.

The lower near logarithmic and the middle uniform portions of the inlet velocity profiles are directly applied from the digitized table of the experimental inputs; provided in Meinders (1998). The upper laminar portion

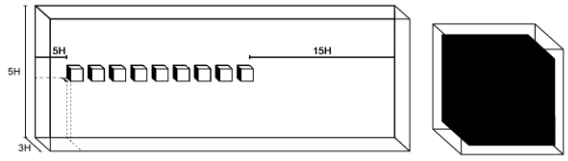

a) *b)*

Figure 6 CFD implementation of the Meinders (1998) experimental setup a) the tunnel chamber b) each cubical shell element

of the profile is obtained in the same manner as mentioned in (Awol et al. 2019). The velocity and turbulent kinetic energy inputs are shown in Figure 7.

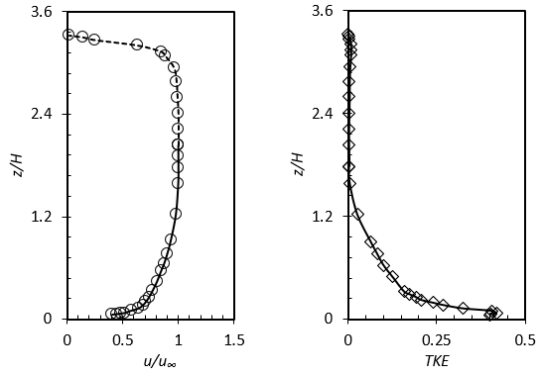

Figure 7 A) The adopted mean inlet velocity and B) turbulent kinetic energy profiles (solid line: data from the experiment; broken line: obtained from re-cycling method; symbol: input implemented in CFD)

A comparison is made against the records of temperature at the surfaces of the 5th cube in the row. The results are collected at the lines of intersection (AB, BC, and CD) between the cube and a longitudinally running vertical plane bisecting the cube, as shown in Figure 8. Liu et al. (2013) conducted the same measurement in a CFD environment with a k-epsilon, k-omega, and LES turbulence models. They found the k-epsilon model to perform better than the other two-equation model (k-omega). The results of the present measurement with Meinders (1998) and Liu et al. (2013), data obtained using the k-epsilon turbulence model, are indicated in Figure 8. On the top and leeward surfaces, the present RSM simulation can predict the experimental results well and better than the k-epsilon turbulence model simulation results. In the windward face, however, both the CFD simulations match but with a margin of error from the experimental records. This may have been due to uncertainty both from spatial coordinate (experimental cube and spacing are very small in size) and temperature measurement itself (Meinders 1998). The artificial introduction of inlet data in the uppermost boundary layer through the method of recycling may have some effects (Awol et al. 2019).

More data has been gathered from a horizontal mid-line on the windward (EF), lateral (FG, HE), and leeward (GH) surfaces of the 5th cube, as shown in Figure 5b; corresponding to the horizontal section plane cutting mid-height of the cubes. The results of this data emphasize the remarks made above.

In general, the present simulation reasonably predicts the temperature distribution on the surface of the building with an average deviation of less than 4 % from the experimental values. Additional information regarding this section can be found from Awol et al. (2019), and Meinders (1998).

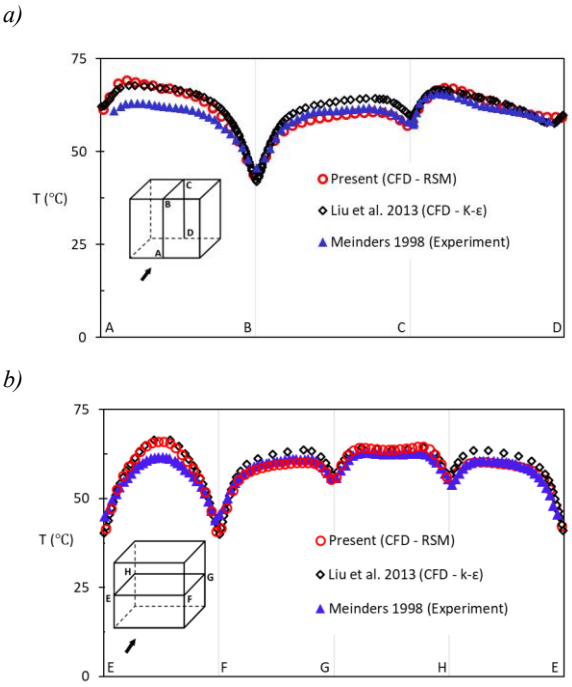

Figure 8 Comparison of simulated and experimental results along the paths: a) ABCD b) EFGHE

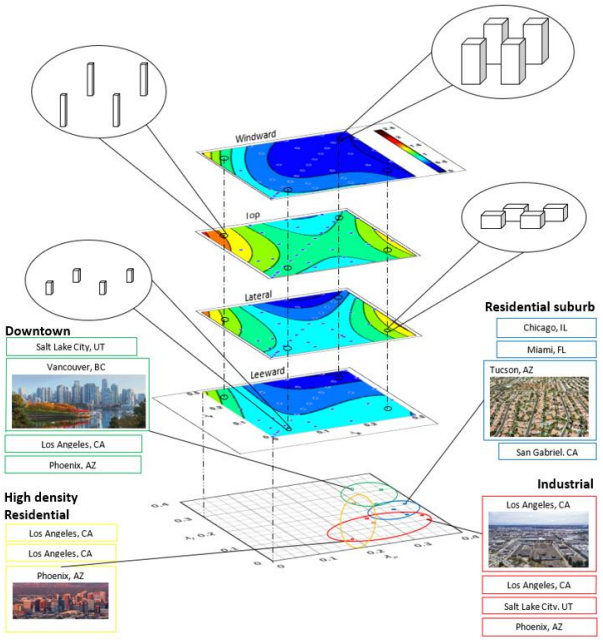

Figure 9 Contour plots of CHTC for each orientation, schematic representation of densities at the extremes, and where the physical urban densities fall

RESULTS AND DISCUSSIONS

The results of the current study are plotted along with the data obtained from the equivalent uniform density (cubical array, Awol et al. 2019) simulations (Figure 9).

CHTC response surface

The results show, for each mean wind speed, that CHTC needs to be viewed as a three-dimensional response surface as a function of planar and frontal densities. The mean CHTC response surfaces for the four orientations of the building, generated from a cubic polynomial interpolation of the simulated data, are shown in Figure 9. The figure indicates a contour plot of the ratio of CHTC at a given canopy density and the CHTC at the isolated building state (h_{dense}/h_{iso}) against the two packing density representations. Figure 9, also, has the schematic representation of four extreme densities, along with the CHTC contours for the four surfaces.

In general, for all surfaces, the highest CHTC value is obtained at a combination of high frontal and low planar density. The Lateral and top surface has additional peak CHTC points near high planar but low frontal densities. The lowest CHTC happens when the highest of the two densities (very dense scenario) overlap. The value of CHTC is found to be intermediate at the combination of low densities from both dimensions (frontal and planar).

The low-planar and high-frontal density combination (isolated slender buildings) give rise to a less disturbed ABL flow in the canopies. The relative slenderness of the obstacles under this scenario makes the tops of the buildings extend into the high velocity portion of the ABL flow. These two may be the reasons why the CHTC is relatively higher under this combination of densities.

Figure 9 shows the least flow space occurs when the density pair (both) become the highest, i.e., large footprint and tall buildings. This is also when the most disturbance to the ABL happens, hence resulting in the lowest mean velocity. This scenario, thus, corresponds to the lowest CHTC. However, there is an additional peak zone for lateral and top surfaces near high-planar and low-frontal density combinations. This corresponds to short but large footprint buildings, with the longest side aligned to along wind direction. As shown in Figure 9, this zone can be described as having corresponded to relatively higher aspect lateral and top surfaces. The relative enlargement of these surfaces means a larger flow attachment region, and consequently, higher convection.

The simulation results also reveal the common claim that the windward surface provides the highest CHTC may not be a general fact. Thus, the windward CHTC contribution may be exceeded by CHTC from other surfaces depending on the density combinations.

The CHTC surface versus Land-use class

The actual planar and frontal densities of neighborhoods from different North American cities have been reported in various literature (Grimmond et al. 1999, Voogt et al. 1997, Burian et al. 2002). The reported data, in general, can be categorized into four land-use class groups, namely; suburban residential, high density residential, industrial, and downtown. The data indicates the most practical range of densities fall in the higher planar, but between low and high frontal densities. Thus, indicating the common assumption to use isolated buildings, and tests in the low planar density zone are less representative of the urban microclimate. The distribution of these densities on a λ_p versus λ_f graph, and their approximate categorization, is as shown in Figure 9.

By corresponding the findings of the present work with the densities of the cites indicated, the density combinations of the cites fall in the range where the lateral and top surfaces contribute the larger CHTC than that of the windward surface.

In addition, Figure 9 may be used to zone CHTC values of buildings based on the built type (land-use class) of the neighborhood. As indicated by the green-colored oval circle, the lowest CHTC values correspond to buildings in downtown, i.e., relatively tall and large footprint structures. The red-colored circle region of low frontal density and mid-to-high planar density corresponds to industrial neighborhoods that have CHTC value comparable or slightly larger than the windward values. These structures are large footprint but low blockage. The high planar density but mid frontal density zone, shown by the blue circle, in between the above two zones refer to the suburban residential neighborhoods. In this region, the CHTC for top and lateral surfaces is larger than that of the windward. The yellow circle near the mid-planar and low-and-mid frontal density range correspond to the mixed residential neighborhoods.

The CHTC surface fit equations

The resulting response surface ($CHTC/h_{iso}$) is fit to a homogeneous bivariate cubic polynomial model, corresponding to "Poly32" in MATLAB. The coefficients of the polynomial are shown in Table 2.

The values of the goodness fit for the surface along all orientations are included. When the polynomial equation (Equation 3) is expressed based on the benchmark case CHTC for the isolated cube, its form is;

$$CHTC = C * u_{10}^{m} * [p_{00} + p_{10}* \lambda_f + p_{01}* \lambda_p + p_{20}*(\lambda_f)^2 + p_{11}* \lambda_f * \lambda_p + p_{02}*(\lambda_p)^2 + p_{30}*(\lambda_f)^3 + p_{21}* (\lambda_f)^2* \lambda_p + p_{12}* \lambda_f *(\lambda_p)^2] \quad (3)$$

Table 2 Coefficients for the polynomials fit for the simulated CHTC data (WW: windward, LW: Leeward, Coeff's: Coefficients)

	Surfaces/orientation			
Coeff's	**WW**	**Top**	**Lateral**	**LW**
p_{00}	0.9551	1.101	0.968	0.914
p_{10}	-4.157	-2.136	0.4681	-1.006
p_{01}	-1.964	3.268	0.1198	-0.7509
p_{20}	38.3	1.366	-14.31	11
p_{11}	-23.65	-15.56	-10.76	-10.16
p_{02}	14.88	-1.962	11.75	10.21
p_{30}	-106.8	30.5	51.28	-35.17
p_{21}	87.75	32.41	100.5	80.58
p_{12}	-36.37	-23.82	-130.5	-87.89
Goodness fit				
SSE	0.00416	0.02538	0.00882	0.01844
R-square	0.9964	0.945	0.9901	0.9728
Adjusted R^2	0.9958	0.9357	0.9884	0.9681
RMSE	0.0094	0.02324	0.0137	0.01981

CONCLUSION

The aim of the current work has been to investigate the effect of broader changes in the urban surface form (built packing density) on the CHTC from surfaces of buildings. Previous studies found the importance of considering the presence of surrounding buildings in the estimation of CHTC from building surfaces in an urban place; through CFD simulation of uniform urban-like cubical obstacles. In this study, the obstacle size is modified to avoid the simplistic but useful approximation of the urban form. The present modification presents a condition of unequal sets of frontal and planar densities.

The results of the study primarily reveal that CHTC is affected both by changes in planar as well as frontal densities. These changes might lead to up to 2.5 times higher or approximately an order of magnitude lower CHTC compared to the conventional U_{10} formulations (h_{iso}, which are mostly done without considering density effects). It is observed the least CHTC values for the windward, and leeward surfaces lie at higher planar densities, whereas the highest CHTC corresponds to the combination of the lowest planar and highest frontal densities. An increase in planar area density increases the CHTC at smaller frontal densities for top and lateral surfaces. The study shows the overall CHTC estimate from conventional models may have mostly been overestimated from the real values in city neighborhoods. Moreover, the general adoption of the windward CHTC as the dominant value among all

surfaces may not be the case at higher planar densities, where most practical city neighborhood densities fall.

This research can be advanced by considering additional heterogeneity in the form of randomness to the urban form and by adopting transitions of density as in changes from the city outskirts to the downtown.

ACKNOWLEDGMENT

The authors would like to acknowledge the SharcNet for providing access to their high-performance computation (HPC) facility and excellent support from their technical staff. The research support from the Ontario Center of Excellence, NSERC Collaborative Research Development, and SOSCIP grants to the first author and Canada Research Chair awards for both the second and the third authors are much appreciated.

Nomenclature

CHTC	Convective heat transfer coefficeint
λ_f	Frontal packing density
λ_p	Planar packing density
$A_{f,i}$	Frontal area per each building
$A_{p,i}$	Planar area per each building
$A_{d,i}$	Unit underlying lot area on the ground surface per each building.
A_F	Total frontal and
A_P	Total top surface areas
A_D	Total lot area
p_{ij}	Coefficeints of the surface fit equation (where *i,j = 0,1,2, or 3)*
h_{iso}	Heat transfer coefficeints from an isolated building study

REFERENCES

Adamek, K., Vasan, N., Elshaer, A., English, E., Bitsuamlak, G.T. 2017. Pedestrian level wind assessment through city development: A study of the financial district in Toronto, Sustainable Cities and Societies, 35:178-190.

Allegrini, J., Dorer, V. Carmeliet, J. 2012. Analysis of convective heat transfer at building façades in street canyons and its influence on the predictions of space cooling demand in buildings, J. Wind Eng. Ind. Aerod. 104:464-473.

Awol, D.A., Bitsuamlak, G.T., Tariku, F. (2019) Numerical estimation of the external convective heat transfer coefficient for buildings in an urban-like setting. Building and Environment 169:106557

Awol, D.A., Bitsuamlak, G.T., Tariku, F. 2017. Consistent analytical urban canopy layer velocity profile for dense building arrangement. Americas Conference on Wind Engineering, Gainsville, United States, 21-24 May 2017

Blocken, B., Defraeye, T. Derome, D. Carmeliet, J. 2009. High-resolution CFD simulations for forced convective heat transfer coefficients at the facade of a low-rise building, Build. Environ. 44:2396-2412.

Blocken, B., Stathopoulos, T., Carmeliet, J., Hensen, J.L.M. 2011. Application of computational fluid dynamics in building performance simulation for the outdoor environment: an overview, Journal of Building Performance Simulation 4:157-184.

Burian, S.J., Velugubantla, S.P., and Brown, M.J. 2002. Morphological analyses using 3D building databases: Phoenix, Arizona. LA-UR-02-6726, Los Alamos National Laboratory, Los Alamos, NM.

Chen, L., Hang, J., Sandberg, M., Claesson, L., Di Sabatino, S., Wigo, H. 2017. The impacts of building height variations and building packing densities on flow adjustment and city breathability in idealized urban models, Build.Environ.; 118:344-361

Cheng, H., Castro, I.P. 2002. Near wall flow over urban-like roughness. Boundary-Layer Meteorol 104(2): 229–259

Coceal, O., Thomas, T.G., Castro, I.P., Belcher, S.E. 2006. Mean flow and turbulence statistics over groups of urban-like cubical obstacles. Boundary-Layer Meteorol 121:491-519

Defraeye, T., Blocken, B., Carmeliet, J. 2011. Convective heat transfer coefficients for exterior building surfaces: Existing correlations and CFD modelling, Energy Conversion and Management 52:512–522

Defraeye, T., Blocken, B., Carmeliet, J. 2010. CFD analysis of convective heat transfer at the surfaces of a cube immersed in a turbulent boundary layer, Int. J. Heat. Mass Transf. 53:297-308.

Emmel, M.G., Abadie, M.O., Mendes, N. 2007. New external convective heat transfer coefficient correlations for isolated low-rise buildings, Energ Build. 39:335-342.

Evangelisti, L., Guattari, C., Gori, P., Bianchi, F. 2017. Heat transfer study of external convective and radiative coefficients for building applications, Energ Build. 151:429–438

Franke, J., Hellsten, A., Schlünzen, H., Carissimo, B. 2011. The COST 732 Best Practice Guideline for CFD simulation of flows in the urban environment: a summary, Int. J. Environ. Pollut. 44 (2011) 419-427.

Grimmond, S. and Oke, T. 1999. "Aerodynamic properties of urban areas derived from analysis of surface form." J. Appl. Met., 38: 1262-1292.

Hagishima, A., Tanimoto, J. (2003) Field measurements for estimating the convective heat transfer coefficient at building surfaces, Build. Environ. 38:873-881.

van Hooff, T., Blocken, B. 2010. On the effect of wind direction and urban surroundings on natural ventilation of a large semi-enclosed stadium, Computers & Fluids 39:1146-1155.

Ito, N., Kimura, K., Oka, J. 1972. Field experiment study on the convective heat transfer coefficient on exterior surface of a building, ASHRAE Trans. 78:184-192.

Kahsay, M.T., Bitsuamlak, G., Tariku, F. (2018) Numerical analysis of convective heat transfer coefficient for building facades, Journal of Building Physics I–23

Launder, B., Reece, G. J., Rodi, W. 1975. Progress in the Development of a Reynolds Stress Turbulence Closure, J Fluid Mech. 68(3):537 – 566

Leschziner, M.A. 1990. Modelling engineering flows with Reynolds stress turbulence closure, J. Wind Eng. Ind. Aerodyn. 35:21-47.

Liu, J. Srebric, J. Yu, N. 2013. Numerical simulation of convective heat transfer coefficients at the external surfaces of building arrays immersed in a turbulent boundary layer, Int. J. Heat. Mass Transf. 61:209-225.

Liu, Y., Harris, D.J. 2007. Full-scale measurements of convective coefficient on external surface of a low-rise building in sheltered conditions, Build. Environ. 42:2718-2736.

Loveday, D.L., Taki, A.H. 1996. Convective heat transfer coefficients at a plane surface on a full-scale building facade, Int. J. Heat. Mass Transf. 39:1729-1742.

Macdonald, R.W. 2000. Modelling the mean velocity profile in the urban canopy layer. Boundary Layer Meteorol 97(1):25–45

Meinders, E.R. 1998. Experimental Study of Heat Transfer in Turbulent Flows over Wall Mounted Cubes, PhD thesis, Technische Universiteit Delft.

Mirsadeghi, M., Costola, D., Blocken, B., Hensen, J.L.M. 2013. Review of external convective heat transfer coefficient models in building energy simulation programs: implementation and uncertainty, Appl. Therm. Eng. 56:134-151.

Montazeri, H. Blocken, B. 2017. New generalized expressions for forced convective heat transfer coefficients at building facades and roofs, Build Environ. 119:153-168

Moonen, P., Defraeye, T., Dorer, V., Blocken, B., Carmeliet, J. 2012. Urban physics: effect of the microclimate on comfort, health and energy demand, Frontiers of Architectural Research 1:197-228.

Murthy, B.N., Joshi, J.B. 2008. Assessment of standard k–e, RSM and LES turbulence models in a baffled stirred vessel agitated by various impeller designs, Chem Eng Sci. 63: 5468 – 5495

Oke, T.R. 1988. Street design and urban canopy layer climate. Energ Build 11(1-3)103-113

Palyvos, J.A. 2008. A survey of wind convection coefficient correlations for building envelope energy systems' modeling, Appl. Therm. Eng. 28:801-808.

Sharples, S. 1984. Full-scale measurements of convective energy losses from exterior building surfaces, Build. Environ. 19:31-39.

Sparrow, E.M., Ramsey, J.W., Mass, E.A. 1979. Effect of finite width on heat transfer and fluid flow about an inclined rectangular plate, J. Heat. Transf. 101:199-204.

Speziale, C.G. 1991. Analytical Methods for the Development of Reynolds-Stress Closures in Turbulence, Annu Rev Fluid Mech., 23:107-157

Tominaga, Y., Mochida, A., Yoshie, R., Kataoka, H., Nozu, T., Yoshikawa, M., Shirasawa, T. 2008. AIJ guidelines for practical applications of CFD to pedestrian wind environment around buildings, J. Wind Eng. Ind. Aerodyn. 96:1749-1761.

Voogt, J. and Oke, T. 1997. "Complete urban surface temperatures." J. Appl. Met., 36: 1117-1132.